

Detecting a long lived false vacuum with quantum quenches

Gianluca Lagnese,^{1,2} Federica Maria Surace,³ Sid Morampudi,⁴ and Frank Wilczek^{4,5,6,7}

¹*Institute of Polar Sciences CNR, Via Torino 155, 30172 Mestre-Venezia, Italy*

²*SISSA, via Bonomea 265, 34136 Trieste, Italy*

³*Department of Physics and Institute for Quantum Information and Matter, California Institute of Technology, Pasadena, California 91125, USA*

⁴*Center for Theoretical Physics, Massachusetts Institute of Technology, Cambridge, MA 02139, USA*

⁵*T. D. Lee Institute and Wilczek Quantum Center, SJTU, Shanghai*

⁶*Arizona State University, Tempe AZ USA*

⁷*Stockholm University Stockholm, Sweden*

(Dated: October 13, 2023)

Distinguishing whether a system supports alternate low-energy (locally stable) states – stable (true vacuum) versus metastable (false vacuum) – by direct observation can be difficult when the lifetime of the state is very long but otherwise unknown. Here we demonstrate, in a tractable model system, that there are physical phenomena on much shorter time scales that can diagnose the difference. Specifically, we study the spectral density following a quench in the tilted quantum Ising model, and show that the evolution of the spectral density is a powerful diagnostic. Small transition bubbles are more common than large ones, and we see characteristic differences in the size dependence of bubble lifetimes even well below the critical size for false vacuum decay. We expect this sort of behavior to be generic in systems of this kind. We show such signatures persist in a continuum field theory. This also opens the possibility of similar signatures of the potential metastable false vacuum of our universe well before the beginning of a decay process to the true vacuum.

Many interesting physical systems, possibly including our present-day universe [1], can exist in metastable states. The decay of a metastable state (or *false vacuum*) is in general understood as a phenomenon of bubble nucleation [2, 3]. The theory of thermal bubble nucleation was introduced in Langer’s pioneering work [2] on Ising ferromagnets and extended to quantum field theory by Kobzarev *et al.* [3]. The quantum version was deeply analyzed in seminal work by Sidney Coleman [4]. In a quantum system, bubbles of true vacuum arise as quantum fluctuations. Most bubbles have a large energy cost associated with the surface tension of their walls, and are therefore transient, or virtual. Bubbles larger than a critical size, on the other hand, can release more energy than is needed to create their walls. Those bubbles will expand indefinitely, at an accelerating rate, and ultimately engulf the entire system. But the time needed to create a super-critical bubble can be extremely long. Can we identify observable signatures testing whether a system – or the universe – is in a false vacuum even if the decay takes an absurdly long time?

The traditional approach to bubble nucleation and false vacuum decay computes the decay rate using a semi-classical approximation [4, 5]. In the limit of small quantum fluctuations, the contribution of the dominant, critical bubble can be isolated by solving a classical evolution in imaginary time. Quantum corrections around the semi-classical solution are then included [6–9]. Recently, motivated by advances in the experimental study of out-of-equilibrium dynamics in many-body quantum systems [10–22], a different method has been used [23–26]. In this method one focuses on real-time evolution af-

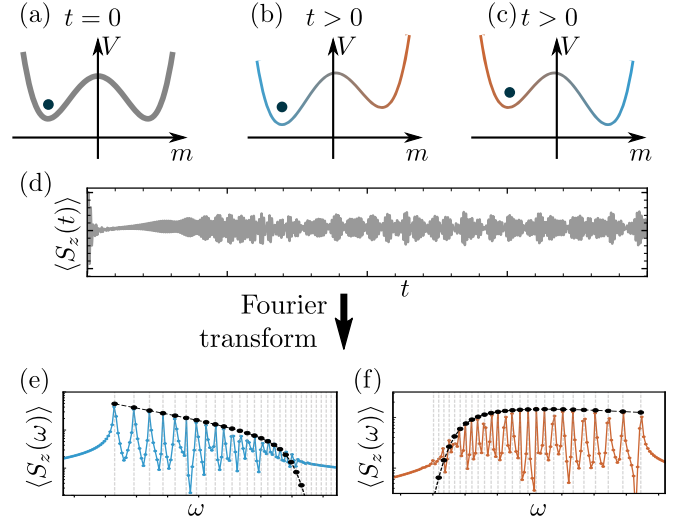


FIG. 1. (a) The system is prepared in one of the degenerate vacua. The Hamiltonian is quenched such that the state of the system is now close (b) to the true vacuum or (c) to a false vacuum. (d) Real-time evolution of the order parameter after the quench. The Fourier transform to the frequency domain reveals whether the systems was in (e) the true vacuum or (f) a false vacuum.

ter a sudden change in some parameters of the theory (a quantum quench [27, 28]). Quantum quenches are now being studied fruitfully in quantum simulators [20, 29–33], and in (classical) numerical simulations using tensor network techniques [34–40]. A parameter of the Hamiltonian is suddenly changed across a first order phase transition such that the previous ground state becomes a false

vacuum. Time evolution starting from this well-defined false vacuum can be studied by measuring the time evolution of suitable observables [41]. In appropriate limits, the traditional results based on semiclassical approaches are recovered. But the post-quench dynamics can reveal much more information, notably including the occurrence and properties of subcritical, “virtual” bubbles: these are off-resonant states in the language of equilibrium perturbation theory, but can be excited in such non-equilibrium setup.

Such bubbles have characteristic dynamical effects at times much shorter than the false vacuum halflife. These effects can be used to distinguish true from false vacuum. Here we demonstrate those claims quantitatively in a tractable model, where (for example) the temporal structure of post-quench oscillations in local observables maps directly onto bubble parameters.

Quench protocol — We consider the transverse field Ising model with a confining longitudinal field, defined by

$$H = - \sum_i [\sigma_i^z \sigma_{i+1}^z - h_z \sigma_i^z - h_x \sigma_i^x]. \quad (1)$$

We initialize the system in the product state $|\psi_\downarrow\rangle$ with spins polarized in the $-\hat{z}$ direction, so that $\langle \psi_\downarrow | \sigma_i^z | \psi_\downarrow \rangle = -1 \forall i$. Then we prepare the ground state for $h_z = 0$ and fixed h_x (with $0 < h_x < 1$) by evolving $|\psi_\downarrow\rangle$ in imaginary time until we reach convergence. The ground state that we obtain is one of the two degenerate ground state of the quantum Ising chain in the ferromagnetic phase, namely the one with negative magnetization, as illustrated in Fig. 1-(a). Subsequently, this state is evolved in real time with either (i) $h_z > 0$, in which case we say we are evolving from the true vacuum $|0_+\rangle$, Fig. 1-(b); or (ii) $h_z < 0$, evolving from the false vacuum $|0_-\rangle$, Fig. 1-(c).

We then compute the magnetization during the real-time evolution, i.e., $\langle S_z(t) \rangle = \sum_i \langle \psi(t) | \sigma_i^z | \psi(t) \rangle / 2N$, where $|\psi(t)\rangle = e^{-iHt} |0_\pm\rangle$ and N is the number of spins in the chain. As shown in Fig. 1-(d), the most evident qualitative behavior is the emergence of distinctive oscillations that clearly distinguish the two cases (i) and (ii) [Fig. 1-(e,f)]. These modes are the main focus of our analysis. In particular, we will analyze the Fourier transform

$$\begin{aligned} S_z(\omega) &= \frac{1}{T} \int_0^T dt \langle S_z(t) \rangle e^{i\omega t} \\ &= \frac{1}{2NT} \sum_i \int_0^T dt \langle \sigma_i^z(t) \rangle e^{i\omega t}. \end{aligned} \quad (2)$$

The procedure outlined here for a quantum Ising chain can be extended to any model possessing a multiple-folded ground state degeneracy: a suitable small symmetry-breaking field is quenched and the time evolution of the corresponding order parameter is examined [42].

Theory — Now we provide a theoretical framework for understanding the post-quench dynamics. For $h_z = 0$ the Hamiltonian can be mapped exactly onto a free-fermion model. We restrict to $0 < h_x < 1$, so that the ground state prepared with imaginary time evolution is one of the ferromagnetic ground states [43]. The dispersion relation of the fermions (*kinks*) is

$$\epsilon(\theta) = 2\sqrt{(1-h_x)^2 + 4h_x \sin^2\left(\frac{\theta}{2}\right)}, \quad (3)$$

where θ is the quasimomentum of the fermion.

Let us turn on a small $h_z \neq 0$. The longitudinal field $V = \sum_i h_z \sigma_i^z$ induces a linear potential that binds the fermionic excitations in pairs [44, 45], and also allows creation and annihilation of pairs of excitations. Following [46], we can split V into two terms. The first, “force” term is obtained by projecting V within sectors with a fixed number of fermions. As we will discuss, this term completely changes the spectrum of the model and must be treated non-perturbatively. The residual interaction, which couples sectors containing different numbers of fermions, can be treated perturbatively. Since $|h_z|$ is much smaller than the mass $\Delta \equiv 2(1-h_x)$ of the fermions, for our purposes we can restrict our attention to the no-particle and two-particle sector, and also study the two terms separately.

Two-particle spectrum — The energy levels in the two-particle sector are obtained by solving the following eigenvalue equation for a pair of fermions with zero center-of-mass momentum (See the Supplemental Material [47] for a derivation.):

$$\sum_{n' \in \mathbb{Z}^+} (K_{n-n'} - K_{n+n'}) \phi_\ell(n') \pm M |h_z| n \phi_\ell(n) = \frac{E_\ell}{2} \phi_\ell(n). \quad (4)$$

Here $n \in \mathbb{Z}^+$ labels the distance between the fermions, $\phi_\ell(n)$ is the eigenfunction with quantum number ℓ , $M = (1-h_x^2)^{1/8}$ is the magnetization, and the hoppings K_r , derived from the free-fermion Hamiltonian, are defined as

$$K_r = \int_{-\pi}^{\pi} \frac{d\theta}{2\pi} \epsilon(\theta) e^{ir\theta}. \quad (5)$$

The quantum number $\ell = 1, 2, \dots$ labels the eigenstates in ascending order with respect to their characteristic inter-particle distance. The plus/minus signs are for the quench from the true/false vacuum respectively. The solutions of Eq. (4) for the “+” sign can be interpreted as *mesons*: they are two-kink bound states that result from the attractive linear potential generated by the longitudinal field; they have positive energy E_ℓ with respect to the ground state, with E_ℓ increasing with ℓ , and they represent the new low-energy excitations of the model. The

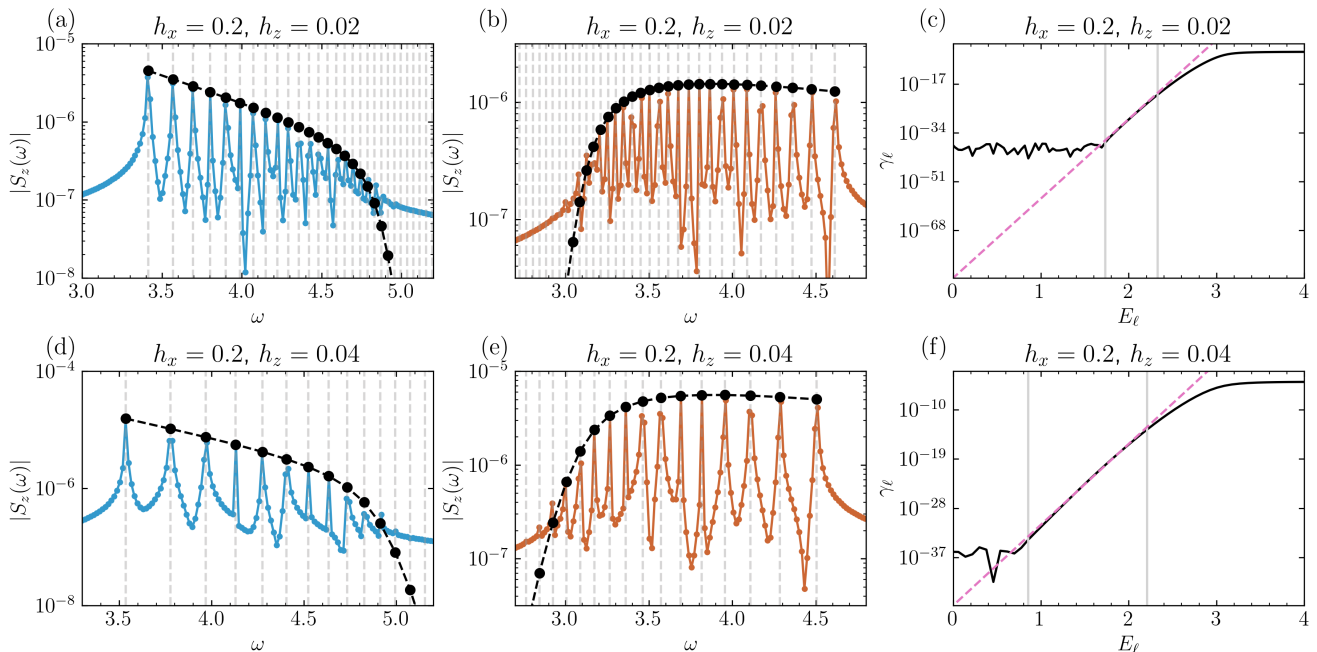


FIG. 2. Fourier transform of the real-time evolved magnetization after a quench from the true vacuum [(a) and (d)] and false vacuum [(b) and (e)]. Parameters are $h_x = 0.2$ and different h_z : in (a) and (b) $h_z = 0.02$, in (d) and (e) $h_z = 0.04$. The Fourier spectrum is compared with the predicted peaks positions E_ℓ and amplitudes $|S^z(\omega = \pm E_\ell)|$ extracted from Eq. (4) and (7). Panels (c) and (f): exponential fitting of the amplitudes of the subcritical bubbles and $E_\ell \rightarrow 0$ extrapolation of the decay rate γ according to Eq. (8).

solutions for the “-” sign are more properly named *bubbles* (though we sometimes use that term in both cases). They can have positive or negative E_ℓ , and, since the interaction is repulsive, E_ℓ decreases with ℓ . The critical bubble ℓ_{res} corresponds to the smallest ℓ such that $E_\ell \leq 0$.

In Fig. 2-(a,d) and Fig. 2-(b,e), we compare the energy levels obtained by solving Eq. (4) with the spectral analysis of $S_z(\omega)$ obtained from iTEBD numerical simulations for the evolution from the true and false vacuum, respectively. The solutions E_ℓ (dashed vertical lines) are in excellent agreement with the frequencies of the modes in $S_z(\omega)$.

Amplitudes — To compute the amplitudes of the oscillations of the magnetization we assume

$$|\psi(t)\rangle \simeq |0_\pm\rangle + \sum_\ell a_\ell(t) e^{-iE_\ell t} |\phi_\ell\rangle, \quad (6)$$

where $|0_\pm\rangle$ is the true/false vacuum and $E_\ell, |\phi_\ell\rangle$ are the two-particle energies and eigenstates from Eq. (4). The coefficients $a_\ell(t)$ depend on the coupling between the vacuum and the two-particle states induced by the perturbation. By evaluating these matrix elements (see the Supplemental Material [47]), we find that the peaks of the Fourier transform $S_z(\omega)$ occur at energies $\pm E_\ell$ with

amplitude

$$|S_z(\omega = \pm E_\ell)| \simeq \frac{|h_z| M^2}{8|E_\ell|} \left(\sum_n h_x^n \phi_\ell(n) \right)^2. \quad (7)$$

In Fig. 2-(a,b,d,e) these theoretical prediction for the amplitudes (black dots) are compared with the amplitudes derived from spectral analysis of the real-time evolved magnetization. We find that within the region where practical limitations on time length and time step allow for clear resolution of the peaks in the spectrum they are remarkably consistent.

Decay rate — Even without a direct observation of the formation of resonant true-vacuum bubbles, it is possible to extrapolate the decay rate of the false vacuum from the peak amplitudes in the magnetization of the non-resonant states. The analytic expression for the decay rate [46, 47] can be approached using the auxiliary quantities

$$\gamma_\ell \equiv 2\pi \frac{|V_\ell|^2}{N} = 4\pi h_z E_\ell |S_z(\omega = E_\ell)|, \quad (8)$$

where $V_\ell = \langle 0_- | V | \phi_\ell \rangle$. The actual decay rate γ , i.e., the probability density per unit time for the critical bubble to be produced, is obtained from Eq. (8) in the limit $E_\ell \rightarrow 0$. This limit can be extrapolated from a suitable exponential fitting of γ_ℓ , as illustrated Fig. 2-(c,f). as a function of the energy level E_ℓ . (For pragmatic reasons, we inserted the theoretical prediction for $S_z(\omega)$ from Eq. (7)

directly into Eq. (8).) The extrapolated exponents of the decay rates are $\log(\gamma) = -196$ for $h_z = 0.02$ [Fig. 2-(c)] and $\log(\gamma) = -108$ for $h_z = 0.04$ [Fig. 2-(f)]. The results are contrasted with the analytical prediction formulated in Ref. [46], which states the decay exponents are $\log(\gamma_{\text{th}}) = -208$ and $\log(\gamma_{\text{th}}) = -104$. Note that such extrapolation shares, by construction, the same underlying assumption behind the computation of the decay rate in Ref. [46] which is known to disagree with other estimates [48, 49] by a constant prefactor (see for instance the discussion in Ref. [24]). Hence, our analysis cannot shed any light on the conflicting results concerning the value of the prefactor.

Importantly, the characteristic time scale of the decay $\tau \approx 1/\gamma$ is much larger than the evolution time $T = 400$ that we use for the iTEBD simulations in Figs. 2-(a,b,d,e). The spectral analysis of the oscillations can therefore probe the stable/metastable nature of the vacuum on time scales that are significantly shorter than the decay time (by many orders of magnitude).

Scaling limit – We now show how to connect our results for the Fourier transform $S_z(\omega)$ to continuum Ising field theory. The lattice model in Eq. (1) has a quantum critical point in $h_x = 1$, $h_z = 0$: in its vicinity, the model scales to the $c = 1/2$ Ising conformal field theory, perturbed by the energy density operator $\epsilon(x)$ (yielding a finite mass m for the kinks) and the spin operator $\sigma(x)$ (as the effect of a longitudinal field h). This field theory depends on the single dimensionless parameter $\eta = m \cdot |h|^{-8/15}$.

To reach the continuum limit from our results for the quantum Ising chain, we rescale the frequency ω in units of the mass gap $\Delta = 2(1 - h_x)$, and the magnetization in units of $M = (1 - h_x^2)^{1/8}$:

$$\tilde{\omega}_\ell \equiv \frac{E_\ell}{\Delta}, \quad \tilde{S}_\ell \equiv \frac{S^z(E_\ell)}{M}. \quad (9)$$

In Fig. 3-(a,b) we plot our results (obtained using Eq. (7)) for values of h_x, h_z increasingly close to the critical point, while keeping the parameter $\tilde{\eta}$ defined by

$$\tilde{\eta} = (2\bar{s})^{8/15} \frac{(1 - h_x)}{(1 + h_x)^{1/15} h_z^{8/15}}, \quad (10)$$

fixed. Here $\bar{s} = 1.35783\dots$. The parameter $\tilde{\eta}$ approximates the dimensionless parameter η of the field theory, and $\tilde{\eta} \rightarrow \eta$ in the scaling limit. We observe that the values of $|\tilde{S}_\ell|$ [Fig. 3-(a,b)] tend to converge to finite values as $h_x \rightarrow 1$ for the case of the true vacuum, and are in good agreement with the results obtained in the continuum using the non-relativistic approximation [47][50]. For the false vacuum, on the other hand, the values of $|\tilde{S}_\ell|$ tend to zero for $h_x \rightarrow 1$. The reason is that, while the spectrum of the mesons remains discrete in the continuous limit, the spectrum of the proper bubbles becomes continuous: the typical gap in the (rescaled) spectrum of the

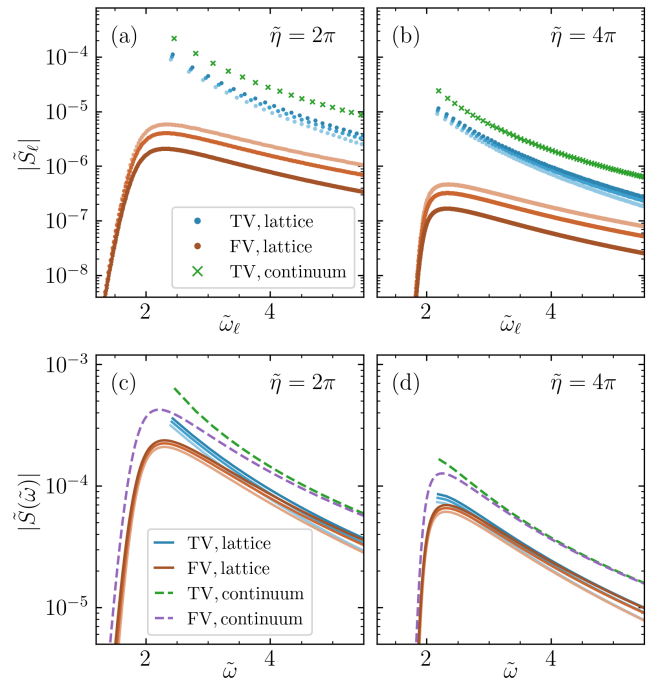


FIG. 3. Scaling limit. Blue/Orange: magnetization spectrum for the lattice models. The intensity of the color represents the closeness to the critical point ($h_x = 0.7, 0.8, 0.9$, from lighter to darker tone). Green/Purple: magnetization spectrum in the continuum for the true/false vacuum within the non-relativistic approximation.

bubbles is $|\tilde{\omega}_\ell - \tilde{\omega}_{\ell-1}| \sim 2h_z M/\Delta = 2\bar{s}\tilde{\eta}^{-15/8}(1 - h_x)$, that goes to zero in the scaling limit. We can obtain the continuous spectrum of the magnetization by an appropriate rescaling bringing in the density of states $\rho(\omega_\ell) \sim (\tilde{\omega}_{\ell+1} - \tilde{\omega}_\ell)^{-1}$:

$$\tilde{\omega}_\ell \rightarrow \tilde{\omega}, \quad \tilde{S}_\ell \cdot (\tilde{\omega}_{\ell+1} - \tilde{\omega}_\ell)^{-1} \rightarrow \tilde{S}(\tilde{\omega}). \quad (11)$$

The plots in Fig. 3-(c,d) show the convergence of $\tilde{S}(\tilde{\omega})$ for the false vacuum.

Observe that the profiles of $\tilde{S}(\tilde{\omega})$ for the two cases (true and false vacuum) tend to coincide for large $\tilde{\eta}$ in the range $\tilde{\omega} \gtrsim 2$. We can understand this as follows. The limit $\eta \rightarrow \infty$ corresponds to the quench with a vanishingly small longitudinal field h (known as *thin wall* limit). In this limit, we recover the standard theory of false vacuum decay: metastability has observable effects only at long times (longer than the inverse of the mass of two kinks), while the short-time dynamics is governed by the free dynamics of the kinks, which are not affected by the very weak confining potential at short times [51]. On the other hand, if η is finite, the dynamics of the magnetization can reveal whether the initial state was the true or the false vacuum. We should remark, however, that our truncation at two fermions precludes accurate treatment of very small η .

Outlook – The spectral analysis performed here for the paradigmatic example of the quantum Ising chain can be applied to probe the presence of a long-lived false vacuum in a very general class of models. In [47], we show how this method allows to detect the signatures of a long-lived false vacuum in a Rydberg atom array on time scales that are experimentally accessible. The issue of discriminating between stability and long-lived metastability arises very generally as one varies parameters in systems that exhibit first-order phase transitions, particularly near the onset and terminal structures of hysteresis curves. We foresee immediate applications of this procedure to other experimental platforms, including ultracold atoms in optical lattices, trapped ions, and superconducting qubits.

A phenomenon that is closely related to the decay of the false vacuum was observed in the string breaking dynamics after a quench in quantum spin chains [35, 52], where the unstable string connecting two charges can persist to very long times. We expect that a similar spectral analysis could help interpret the real-time evolution observed in these works.

Promising directions include, moreover, the study of metastable phases of matter and their dynamical preparation. A metastable quantum spin liquid phase could explain, for example, the features recently observed in a Rydberg-atom quantum simulator in two spatial dimensions [53–55].

In the one-dimensional system we focused on here, the boundary between true and false vacuum is marked by zero-dimensional structures, i.e., particle-like “domain walls”. In higher dimensions the boundaries will be extended objects, having significant low-energy internal degrees of freedom, notably including variables that encode their shapes. In two and three dimensions the boundaries of near-critical bubbles will be long-lived strings and membranes respectively. Although directly accessing these objects through simple quenching can be challenging, studying smaller, more accessible bubbles should allow us to gain valuable insights into their properties.

Also worthy of exploration is the possibility of more structured quenches. For definiteness, let us consider again an Ising ferromagnet, starting with the ground state having global magnetization downward, where our destabilizing quench consists of turning on a small field favoring upward magnetization. If at the same time we also flip the spins within a geometrically defined region (or several such), we can encourage the production of large bubbles. We could also flip only a fraction of the spins, to match the desired magnetization, or other refinements. Systematic study and use of this “bubble seeding” concept is evidently not restricted to the Ising ferromagnet, and opens a wide field for investigation.

Expanding bubble walls implement time-dependent boundary conditions for external fields on an accelerating surface. Thus they implement the sort of “moving mir-

ror” boundary conditions that have been widely proposed as idealizations of black hole horizons, specifically in connection with Hawking radiation. Here, since the analog horizon moves outward, we come upon a wide class of accessible *white* holes. (Collapsing bubbles are the black hole analogs.) This concept can be taken much further, as we shall report elsewhere.

Finally let us remark that in a cosmological context differences between scalar-induced energy densities (“cosmological constant” or “dark energy”) introduces a new feature: regions with higher energy density expand faster. It has long been known that this phenomenon can stabilize otherwise unstable vacua [56], roughly speaking by enabling more rapid expansion to outpace bubble expansion; indeed, this presented a serious difficulty for early models of inflation [57]. It will be interesting to explore consequences of this new feature for the signatures dynamics discussed here.

Acknowledgments – We acknowledge useful discussions with A. Bastianello, P. Calabrese, S. B. Rutkevich, and G. Takács.

FMS acknowledges support provided by the U.S. Department of Energy Office of Science, Office of Advanced Scientific Computing Research, (DE-SC0020290), by Amazon Web Services, AWS Quantum Program, and by the DOE QuantISED program through the theory consortium “Intersections of QIS and Theoretical Particle Physics” at Fermilab. FW is supported by the U.S. Department of Energy under grant Contract Number DE-SC0012567, by the European Research Council under grant 742104, and by the Swedish Research Council under Contract No. 335-2014-7424.

-
- [1] J. Elias-Miró, J. R. Espinosa, G. F. Giudice, G. Isidori, A. Riotto, and A. Strumia, Higgs mass implications on the stability of the electroweak vacuum, *Physics Letters B* **709**, 222 (2012).
 - [2] J. Langer, Theory of the condensation point, *Annals of Physics* **41**, 108 (1967).
 - [3] I. Y. Kobzarev, L. B. Okun, and M. B. Voloshin, Bubbles in Metastable Vacuum, *Yad. Fiz.* **20**, 1229 (1974).
 - [4] S. Coleman, Fate of the false vacuum: Semiclassical theory, *Phys. Rev. D* **15**, 2929 (1977).
 - [5] S. Coleman, The uses of instantons, in *The Whys of Subnuclear Physics*, edited by A. Zichichi (Springer US, Boston, MA, 1979) pp. 805–941.
 - [6] C. G. Callan, Jr. and S. R. Coleman, The Fate of the False Vacuum. 2. First Quantum Corrections, *Phys. Rev. D* **16**, 1762 (1977).
 - [7] A. Andreassen, D. Farhi, W. Frost, and M. D. Schwartz, Direct approach to quantum tunneling, *Phys. Rev. Lett.* **117**, 231601 (2016).
 - [8] A. Andreassen, D. Farhi, W. Frost, and M. D. Schwartz, Precision decay rate calculations in quantum field theory, *Phys. Rev. D* **95**, 085011 (2017).
 - [9] A. Ivanov, M. Matteini, M. Nemevšek, and L. Ubaldi,

- Analytic thin wall false vacuum decay rate, *Journal of High Energy Physics* **2022**, 209 (2022).
- [10] S. Hofferberth, I. Lesanovsky, B. Fischer, T. Schumm, and J. Schmiedmayer, Non-equilibrium coherence dynamics in one-dimensional Bose gases, *Nature* **449**, 324 (2007).
- [11] S. Trotzky, Y.-A. Chen, A. Flesch, I. P. McCulloch, U. Schollwöck, J. Eisert, and I. Bloch, Probing the relaxation towards equilibrium in an isolated strongly correlated one-dimensional Bose gas, *Nature Physics* **8**, 325 (2012).
- [12] M. Gring, M. Kuhnert, T. Langen, T. Kitagawa, B. Rauer, M. Schreitl, I. Mazets, D. A. Smith, E. Demler, and J. Schmiedmayer, Relaxation and Prethermalization in an Isolated Quantum System, *Science* **337**, 1318 (2012).
- [13] M. Cheneau, P. Barmettler, D. Poletti, M. Endres, P. Schauß, T. Fukuhara, C. Gross, I. Bloch, C. Kollath, and S. Kuhr, Light-cone-like spreading of correlations in a quantum many-body system, *Nature* **481**, 484 (2012).
- [14] F. Meinert, M. J. Mark, E. Kirilov, K. Lauber, P. Weinmann, A. J. Daley, and H.-C. Nägerl, Quantum Quench in an Atomic One-Dimensional Ising Chain, *Phys. Rev. Lett.* **111**, 053003 (2013).
- [15] T. Langen, R. Geiger, M. Kuhnert, B. Rauer, and J. Schmiedmayer, Local emergence of thermal correlations in an isolated quantum many-body system, *Nature Physics* **9**, 640 (2013).
- [16] M. Schreiber, S. S. Hodgman, P. Bordia, H. P. Lüschen, M. H. Fischer, R. Vosk, E. Altman, U. Schneider, and I. Bloch, Observation of many-body localization of interacting fermions in a quasirandom optical lattice, *Science* **349**, 842 (2015).
- [17] T. Langen, S. Erne, R. Geiger, B. Rauer, T. Schweigler, M. Kuhnert, W. Rohringer, I. E. Mazets, T. Gasenzer, and J. Schmiedmayer, Experimental observation of a generalized Gibbs ensemble, *Science* **348**, 207 (2015).
- [18] A. M. Kaufman, M. E. Tai, A. Lukin, M. Rispoli, R. Schittko, P. M. Preiss, and M. Greiner, Quantum thermalization through entanglement in an isolated many-body system, *Science* **353**, 794 (2016).
- [19] T. Fukuhara, P. Schauß, M. Endres, S. Hild, M. Cheneau, I. Bloch, and C. Gross, Microscopic observation of magnon bound states and their dynamics, *Nature* **502**, 76 (2013).
- [20] H. Bernien, S. Schwartz, A. Keesling, H. Levine, A. Omran, H. Pichler, S. Choi, A. S. Zibrov, M. Endres, M. Greiner, V. Vuletić, and M. D. Lukin, Probing many-body dynamics on a 51-Atom quantum simulator, *Nature* **551**, 579 (2017).
- [21] J. Zhang, G. Pagano, P. W. Hess, A. Kyprianidis, P. Becker, H. Kaplan, A. V. Gorshkov, Z.-X. Gong, and C. Monroe, Observation of a many-body dynamical phase transition with a 53-qubit quantum simulator, *Nature* **551**, 601 (2017).
- [22] D. Bluvstein, A. Omran, H. Levine, A. Keesling, G. Semeghini, S. Ebadi, T. T. Wang, A. A. Michailidis, N. Maskara, W. W. Ho, et al., Controlling quantum many-body dynamics in driven Rydberg atom arrays, *Science* **371**, 1355 (2021).
- [23] G. Lagnese, F. M. Surace, M. Kormos, and P. Calabrese, False vacuum decay in quantum spin chains, *Phys. Rev. B* **104**, L201106 (2021).
- [24] D. Szász-Schagrin and G. Takács, False vacuum decay in the $(1+1)$ -dimensional φ^4 theory, *Phys. Rev. D* **106**, 025008 (2022).
- [25] O. Pomponio, M. A. Werner, G. Zarand, and G. Takacs, Bloch oscillations and the lack of the decay of the false vacuum in a one-dimensional quantum spin chain, *SciPost Phys.* **12**, 061 (2022).
- [26] M. Lencsés, G. Mussardo, and G. Takács, Variations on vacuum decay: The scaling Ising and tricritical Ising field theories, *Phys. Rev. D* **106**, 105003 (2022).
- [27] P. Calabrese and J. Cardy, Time dependence of correlation functions following a quantum quench, *Phys. Rev. Lett.* **96**, 136801 (2006).
- [28] P. Calabrese and J. Cardy, Quantum quenches in extended systems, *Journal of Statistical Mechanics: Theory and Experiment* **2007**, P06008 (2007).
- [29] F. M. Surace, P. P. Mazza, G. Giudici, A. Lerose, A. Gambassi, and M. Dalmonte, Lattice Gauge Theories and String Dynamics in Rydberg Atom Quantum Simulators, *Phys. Rev. X* **10**, 021041 (2020).
- [30] D. Banerjee, M. Dalmonte, M. Müller, E. Rico, P. Stebler, U.-J. Wiese, and P. Zoller, Atomic quantum simulation of dynamical gauge fields coupled to fermionic matter: From string breaking to evolution after a quench, *Phys. Rev. Lett.* **109**, 175302 (2012).
- [31] J. Vovrosh and J. Knolle, Confinement and entanglement dynamics on a digital quantum computer, *Scientific reports* **11**, 11577 (2021).
- [32] W. L. Tan, P. Becker, F. Liu, G. Pagano, K. Collins, A. De, L. Feng, H. Kaplan, A. Kyprianidis, R. Lundgren, et al., Domain-wall confinement and dynamics in a quantum simulator, *Nature Physics* **17**, 742 (2021).
- [33] A. Zenesini, A. Berti, R. Cominotti, C. Rogora, I. G. Moss, T. P. Billam, I. Carusotto, G. Lamporesi, A. Recati, and G. Ferrari, Observation of false vacuum decay via bubble formation in ferromagnetic superfluids, arXiv preprint arXiv:2305.05225 <https://doi.org/10.48550/arXiv.2305.05225> (2023).
- [34] M. Kormos, M. Collura, G. Takács, and P. Calabrese, Real-time confinement following a quantum quench to a non-integrable model, *Nature Physics* **13**, 246 (2017).
- [35] A. Lerose, F. M. Surace, P. P. Mazza, G. Perfetto, M. Collura, and A. Gambassi, Quasilocalized dynamics from confinement of quantum excitations, *Phys. Rev. B* **102**, 041118 (2020).
- [36] G. Lagnese, F. M. Surace, M. Kormos, and P. Calabrese, Quenches and confinement in a Heisenberg–Ising spin ladder, *Journal of Physics A: Mathematical and Theoretical* **55**, 124003 (2022).
- [37] S. Birnkammer, A. Bastianello, and M. Knap, Prethermalization in one-dimensional quantum many-body systems with confinement, *Nature Commun.* **13**, 7663 (2022).
- [38] S. Scopa, P. Calabrese, and A. Bastianello, Entanglement dynamics in confining spin chains, *Phys. Rev. B* **105**, 125413 (2022).
- [39] A. Milsted, J. Liu, J. Preskill, and G. Vidal, Collisions of false-vacuum bubble walls in a quantum spin chain, *PRX Quantum* **3**, 020316 (2022).
- [40] J. Maki, A. Berti, I. Carusotto, and A. Biella, Monte carlo matrix-product-state approach to the false vacuum decay in the monitored quantum Ising chain, arXiv preprint arXiv:2306.01067 <https://doi.org/10.48550/arXiv.2306.01067> (2023).
- [41] G. Delfino and M. Sorba, Quantum quenches from an

- excited state, *Nuclear Physics B* **994**, 116312 (2023).
- [42] Note that an underlying symmetry is not strictly required: the same analysis can be applied near a first order phase transition. In that case, any parameter that can be used to tune across the phase transition plays the role of the symmetry-breaking field.
- [43] When using finite size methods, one must also include a small longitudinal field in order to avoid creating a cat state.
- [44] B. M. McCoy and T. T. Wu, Two-dimensional ising field theory in a magnetic field: Breakup of the cut in the two-point function, *Phys. Rev. D* **18**, 1259 (1978).
- [45] G. Delfino, G. Mussardo, and P. Simonetti, Non-integrable quantum field theories as perturbations of certain integrable models, *Nuclear Physics B* **473**, 469 (1996).
- [46] S. B. Rutkevich, Decay of the metastable phase in $d = 1$ and $d = 2$ ising models, *Phys. Rev. B* **60**, 14525 (1999).
- [47] Supplemental Material, attached..
- [48] M. B. Voloshin, [Decay of false vacuum in \(1+1\) dimensions](#), Tech. Rep. (USSR, 1985) ITEP-8(1985).
- [49] P. Fonseca and A. Zamolodchikov, Ising field theory in a magnetic field: analytic properties of the free energy (2001), [arXiv:hep-th/0112167 \[hep-th\]](#).
- [50] Our methods rely on the non-relativistic approximation and the two-fermion Hamiltonian truncation. Note that more accurate predictions for the post-quench dynamics in the continuum can be obtained using efficient numerical methods such as the Truncated Fermionic Space Approach (TFSA) [58].
- [51] Note that the mesonic spectrum becomes continuous in the limit $\eta \rightarrow \infty$ [59].
- [52] R. Verdel, G.-Y. Zhu, and M. Heyl, Dynamical localization transition of string breaking in quantum spin chains, arXiv preprint arXiv:2304.12957 <https://doi.org/10.48550/arXiv.2304.12957> (2023).
- [53] G. Semeghini, H. Levine, A. Keesling, S. Ebadi, T. T. Wang, D. Bluvstein, R. Verresen, H. Pichler, M. Kalinowski, R. Samajdar, et al., Probing topological spin liquids on a programmable quantum simulator, *Science* **374**, 1242 (2021).
- [54] G. Giudici, M. D. Lukin, and H. Pichler, Dynamical preparation of quantum spin liquids in rydberg atom arrays, *Phys. Rev. Lett.* **129**, 090401 (2022).
- [55] R. Sahay, A. Vishwanath, and R. Verresen, Quantum spin puddles and lakes: Nisq-era spin liquids from non-equilibrium dynamics, arXiv preprint arXiv:2211.01381 <https://doi.org/10.48550/arXiv.2211.01381> (2022).
- [56] S. Coleman and F. De Luccia, Gravitational effects on and of vacuum decay, *Phys. Rev. D* **21**, 3305 (1980).
- [57] A. H. Guth, Inflationary universe: A possible solution to the horizon and flatness problems, *Phys. Rev. D* **23**, 347 (1981).
- [58] T. Rakovszky, M. Mestyán, M. Collura, M. Kormos, and G. Takács, Hamiltonian truncation approach to quenches in the ising field theory, *Nuclear Physics B* **911**, 805 (2016).
- [59] P. Fonseca and A. Zamolodchikov, Ising Spectroscopy I: Mesons at $T < T_c$, arXiv preprint hep-th/0612304 <https://doi.org/10.48550/arXiv.hep-th/0612304> (2006).